2009 American Control Conference
Hyatt Regency Riverfront, St. Louis, MO, USA
June 10-12, 2009

Modeling and torque estimation of an automotive Dual Mass Flywheel

Ulf Schaper, Oliver Sawodny, Tobias Mahl and Uli Blessing

Abstract— **The Dual Mass Flywheel (DMF) is primarily used for dampening of oscillations in automotive powertrains and to prevent gearbox rattling. This paper explains the DMF mechanics along with its application and components. Afterwards a detailed ab-initio model of the DMF dynamics is presented. This mainly includes a model for the two arc springs in the DMF and their friction behavior. Both centrifugal effects and redirection forces act radially on the arc spring which induces friction. A numerical simulation of the DMF model is compared to measurements for model validation. Finally the observability of the engine torque using the DMF is discussed. For this purpose a linear torque observer is proposed and evaluated.**

I. INTRODUCTION

In today's world powertrain control systems need accurate torque information to perform various tasks. These tasks include for example the clutch actuation in automated manual transmissions (AMTs) and dual-clutch transmissions (DCTs) as well as the control of electric motors in hybrid powertrains. An indirect torque estimation is needed because the direct measurement of the transmitted torque using strain gages cannot be done in volume production cars for economic reasons.

One source for a powertrain torque estimation is the engine itself. However, the torque estimation provided by the internal combustion engine is based on complex thermodynamic models. These engine models tend not to be reliable in all situations. Critical aspects include the accuracy of the turbo charger models and the influence of exhaust gas recirculation on combustion calculation.

In this paper, the possibility of torque estimation using the Dual Mass Flywheel is analyzed. Section II gives a short introduction to the Dual Mass Flywheel and its original use. In section III, the main physical effects are explained and later modeled in section IV. After validating the model using measurement data in section V, the observability of the powertrain torque using speed sensor measurements is discussed in section VI. A linear observer is proposed.

Some work has already been published on modeling the Dual Mass Flywheel without the aim of torque observation. Especially [1] can be recommended as a helpful source. An English summary of [1] can be found in [2]. Further explanations are given in [3]–[6]. Taking a different approach, [7] gives an analysis of the frequency behavior of the DMF. In [8], the DMF is used to detect engine misfire which is similar to powertrain torque observation.

This work was supported by GETRAG, Untergruppenbach.

U. Schaper is studying Engineering Cybernetics at the University of Stuttgart, ulfschaper@gmx.de.

Prof. Dr.-Ing. O. Sawodny and T. Mahl are with the Institute of System Dynamics, University of Stuttgart, 70569 Stuttgart, Germany, {sawodny|mahl}@isys.uni-stuttgart.de.

U. Blessing is Supervisor Software Basics at GETRAG, uli.blessing@getrag.de.

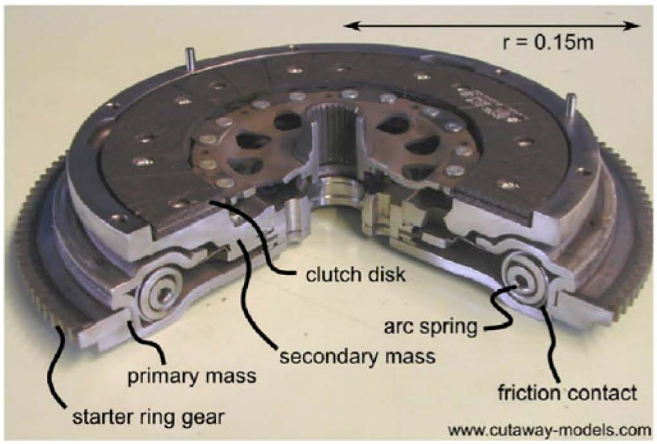

Fig. 1. Photo of a Dual Mass Flywheel, by courtesy of Grau Schnittmodelle, Notzingen, Germany.

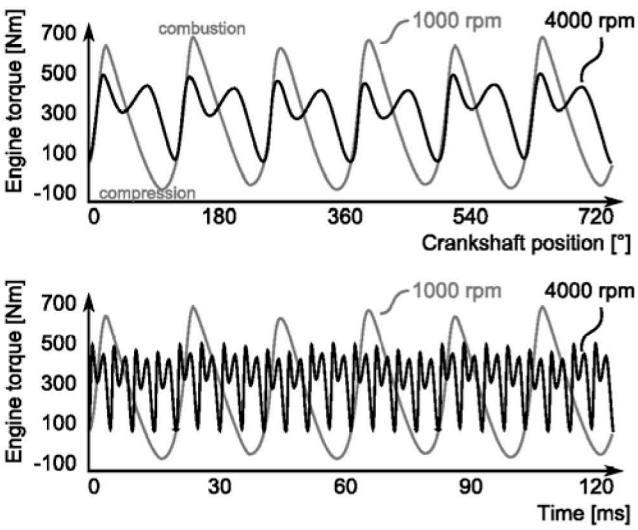

Fig. 2. Filtered engine torque plotted (a) against crankshaft angle and (b) against time for two different engine speeds (measurement data: GETRAG).

II. ORIGINAL PURPOSE OF THE DMF

Piston engines do not generate a constant torque but a time-varying torque $T_{\text{eng}}(t)$. The shape of this torque function depends mainly on the engine speed $\dot{\varphi}_{\text{eng}}$ and the number of cylinders. In Fig. 2(a), the engine torque is plotted over the crankshaft angle using two different levels of engine speed.

The illustrated torque behavior is not directly applicable to a gearbox as it would cause heavy rattling due to the

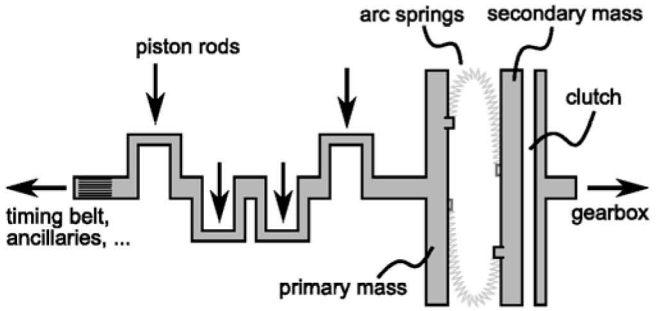

Fig. 3. Crankshaft of 4-cylinder engine with attached Dual Mass Flywheel and clutch disk.

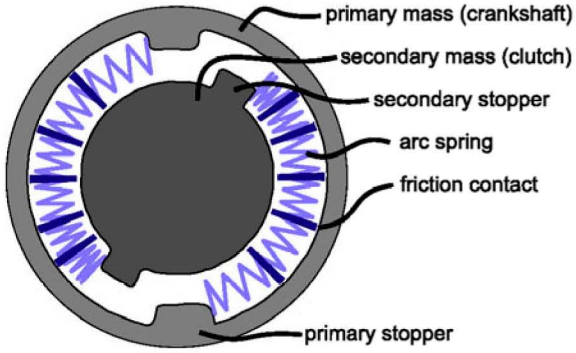

Fig. 4. Simplified sketch of the DMF with compressed springs.

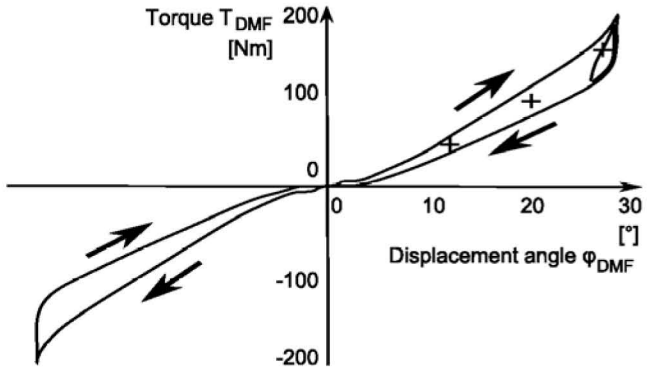

Fig. 5. Torsion experiment with fixed primary mass (data source: GETRAG).

gearwheel teeth clashing back and forth.

The torque progress within two engine rotations can be seen in Fig. 2(a). Each of the six cylinders contributes initially a significant negative torque during its compression stroke. Afterwards, each cylinder returns a positive torque within its power stroke. At higher engine speed levels (such as 4000 1/min) inertial forces become more and more significant. As any piston has to be accelerated and decelerated twice within one engine cycle, the mass forces have a higher frequency than the gas pressure cycles from the combustion process. The effect of the mass forces can be seen in the 4000 1/min plot of Fig. 2(a). Another more obvious impact of the engine speed is the frequency of the combustion cycle itself. At a higher rotation rate, all strokes are faster. Therefore, the frequency of the torque oscillations also rises (see time plot in Fig. 2(b)).

The crankshaft and other mechanical parts of the engine will only dampen high frequency oscillations in the engine torque by themselves. Therefore, low frequencies which occur at low engine speeds have to be dampened by additional design elements. In most cars a solid flywheel is used as a damper. For more demanding applications, the Dual Mass Flywheel has been constructed as a mechanical torsional damping device.

1) Torque oscillation dampening using solid flywheels: In most cars large flywheels are attached to the crankshafts. They have a first-order-lag dynamic behavior. A large inertia is needed to get sufficient dampening at low engine speeds. As a high inertia on the crankshaft delays the engine response to input changes, solid flywheels are not suited for mid-range, luxury class and sporty cars.

2) The Dual Mass Flywheel: In a DMF design, the flywheel inertia is split up into two parts: the primary mass is still attached to the crankshaft while the secondary mass belongs to the clutch (see Fig. 3). Both masses have two small stoppers, each one able to pick up the two arc springs (see Fig. 4). As the arc springs are deflected within the arc channel, they transfer torque from one flywheel to the other. When the arc springs slide through their channel, friction adds dampening characteristics to the Dual Mass Flywheel.

III. PHYSICAL BEHAVIOR OF THE DMF

In this section two torsion experiments are presented. The main effects observed in these experiments will be modeled afterwards.

A. DMF torsion experiment at standstill

The first torsion experiment is done at standstill. That implies that the primary mass is fixed while the secondary mass is slowly rotating. Fig. 5 shows the transmitted torque over the displacement angle.

Since the arc springs are compressed during the torsion experiment, the roughly linear relationship between the displacement angle φ_{DMF} and the transmitted torque T_{DMF} is expected.

However, there are hysteresis losses in the DMF. During decompression, the DMF returns less torque than it needs for being compressed. In Fig. 5, the area between both branches of the hysteresis loop shows the friction energy which is lost within the shown load reversal. It can be seen that the friction torque rises with the displacement angle. The reason for these friction effects are redirection forces. These redirection forces act radially on the springs once the springs transmit tangential forces (from one end to the other). The redirection forces grow with rising elastic spring forces (see Fig. 6(a)).

B. Torsion experiment at higher speeds

The second torsion experiment is similar to the first one, except the primary mass is not fixed. Instead, the primary mass rotates with a constant speed. The second flywheel also adopts this base speed with slight variations in order to achieve displacement angles similar to the experiment before.

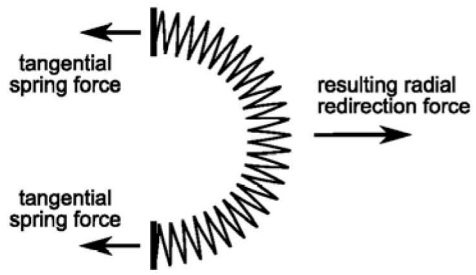

(a) Radial forces due to spring redirection

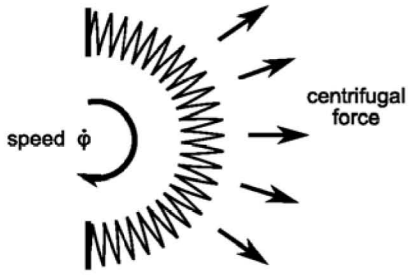

(b) Radial forces due to centrifugal effects

Fig. 6. Two sources for radial contact forces that act on the arc springs

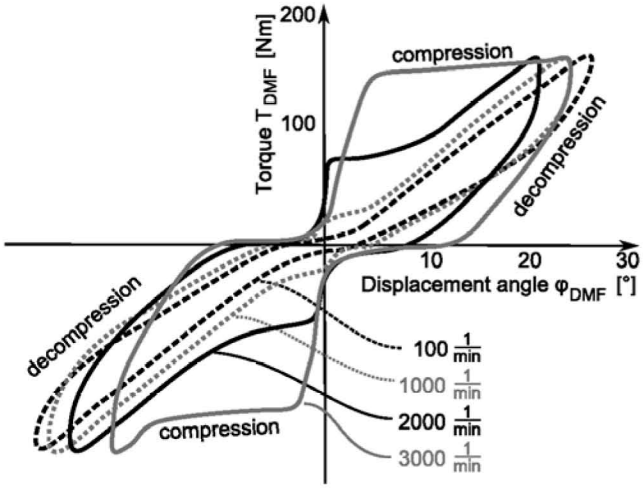

Fig. 7. Torsion experiments at different engine speeds. Source: [1].

Fig. 7 shows the result of this torsion experiment for various speed levels. At an engine speed of 100 1/min the behavior is still very similar to the standstill experiment. However, increasing the speed increases the friction. The reason for this behavior is the radial centrifugal force, which presses the arc spring against the outer casing of the Dual Mass Flywheel (see Fig. 6(b)). The tangential friction forces are directly dependent on these radial contact forces.

In the plots showing experiments done at speed levels of 2000 1/min and 3000 1/min one can even see that the torque stays constant for a wide range of angles and suddenly jumps at about $\varphi_{DMF} = 0°$. The reason for this behavior are stiction effects: At small displacement angles the elastic spring forces are so small that they cannot overcome the friction due to centrifugal force. This results in compressed

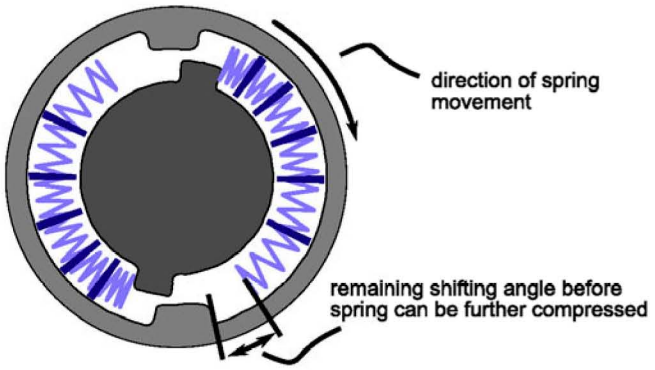

Fig. 8. DMF with the compressed springs being shifted through the channel.

arc springs lying in the spring channel. As long as the stopper of the secondary flywheel is not in contact with this spring, no torque is transmitted. Once the stopper touches the (still compressed) spring, the full spring torque will be transmitted to the stopper. However, as the spring is not extended to full length, moving the stopper into the spring will not result in additional compression but just in shifting the spring within the spring channel (see Fig. 8). Within this phase, the transmitted torque is approximately constant (see Fig. 7).

But even during the operation phases when the springs are properly compressed and relaxed, Fig. 7 shows differences to the standstill experiment from section III-A. The spring stiffness itself depends on the rotation speed: at higher speeds, the decompression straights get steeper. This is due to the fact that the springs are not shortened homogeneously when being compressed, but tend to tense tighter near the stopper of the secondary flywheel. If they do not compress homogeneously, the effective lengths of the springs are shorter, and therefore the stiffness rises.

IV. MODELING OF THE DUAL MASS FLYWHEEL

This section will discuss a model to simulate the physical effects found in section III. At first, a simple model for the flywheels themselves is set up. Afterwards a more complex model for the springs is presented, considering only one of the springs as the other one behaves symmetrically.

A. Flywheel model

In (1) the law of conservation of angular momentum for the primary flywheel is presented. The primary flywheel is modeled as a lumped mass with the moment of inertia J_{pri} and the angular acceleration $\ddot{\varphi}_{pri}$. Analogously J_{sec} denotes the moment of inertia of the secondary flywheel in equation (2) while $\ddot{\varphi}_{DMF}$ is the relative acceleration of the secondary flywheel compared to the first one:

$$J_{pri}\,\ddot{\varphi}_{pri} = \quad T_{eng} - \sigma_1^P\, T_{S,1} + \sigma_6^P\, T_{S,6} + T_{fric,pri} \tag{1}$$

$$J_{sec}\,(\ddot{\varphi}_{pri} + \ddot{\varphi}_{DMF}) = -T_{clu} - \sigma_1^S\, T_{S,1} + \sigma_6^S\, T_{S,6} + T_{fric,sec}. \tag{2}$$

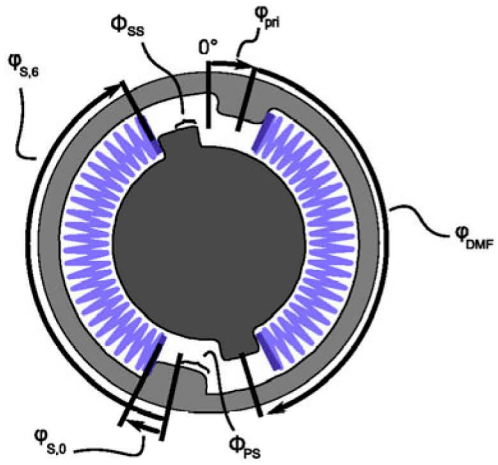

Fig. 9. Coordinate systems for flywheel and spring model. Φ_* denotes constants while φ_* are variable angles. Note that only one spring is modeled, although both springs are used for notational purposes here.

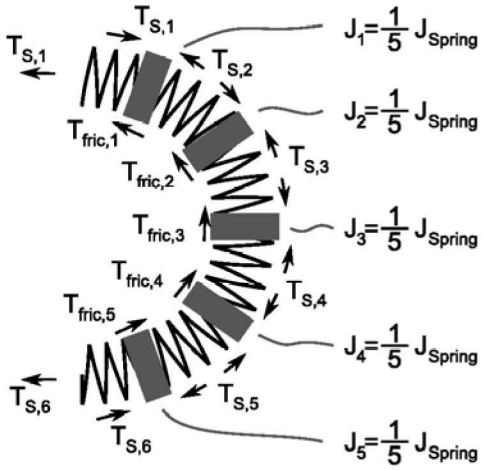

Fig. 10. Spring model with five mass points and six stiffnesses.

In equation (1) and (2), T_{eng} and T_{clu} are the torques of the engine and the clutch respectively. $T_{\text{S},1}$ and $T_{\text{S},6}$ are the spring torques (see section IV-B). Those contribute angular momentum to the flywheels according to the switching functions σ_1^{P}, σ_1^{S}, σ_6^{P} and σ_6^{S}. The torque terms $T_{\text{fric,pri}}$ and $T_{\text{fric,sec}}$ describe all friction forces that act on the flywheels.

The four switching functions $\sigma_*^* \in \{0,1\}$ are $\sigma_*^* = 1$ if the spring is in contact with one of the stoppers of the flywheels. This is the normal case. Otherwise, if the spring is nonattached, the corresponding switching function is set to $\sigma_*^* = 0$. In more detail, if the front end of the spring touches the primary mass stopper, then $\sigma_1^{\text{P}} = 1$. If the spring's back end touches the other primary stopper, then $\sigma_6^{\text{P}} = 1$. Analogously, if the front end of the spring touches the secondary mass, then $\sigma_1^{\text{S}} = 1$. Finally, if the back end of the spring contacts the secondary mass stopper, then $\sigma_6^{\text{S}} = 1$.

Concerning the friction terms $T_{\text{fric,pri}}$ and $T_{\text{fric,sec}}$, two effects have to be modeled: Some friction occurs in the bearings and sealings between both flywheels. This friction torque T_{seal} acts on both flywheels. However, more important is the friction $T_{\text{fric},i}$ (see next section) which results from the springs radial forces. As the DMF casing belongs to the primary flywheel, these friction torques only act on $T_{\text{fric,pri}}$:

$$T_{\text{fric,pri}} = T_{\text{seal}} + \sum_{i=1}^{5} T_{\text{fric},i} \tag{3}$$

$$T_{\text{fric,sec}} = -T_{\text{seal}}. \tag{4}$$

B. Spring model

It is not sufficient to have a homogeneous spring model as it would not show a changing stiffness (see section III-B). Therefore, the spring is fragmented into six elastic segments and five lumped masses [1] (see Fig. 10). Applying the law of angular momentum conservation to these masses returns the simulation equalities ($i = 1 \dots 5$):

$$J_i \left(\ddot{\varphi}_{\text{pri}} + \ddot{\varphi}_{\text{S},i}\right) = \underbrace{T_{\text{S},i} - T_{\text{S},(i+1)}}_{T_{\text{aff},i}} - T_{\text{fric},i}, \tag{5}$$

where the adjacent spring torques $T_{\text{S},i}$ and $T_{\text{S},(i+1)}$ can assumed to be linear. By defining the spring stiffnesses c_i and nominal spring lengths $\Phi_{\text{nom},i}$ ($i = 1 \dots 6$), the spring torques can be computed as:

$$T_{\text{S},i} = c_i \left(\Phi_{\text{nom},i} - \varphi_{\text{S},i} + \varphi_{\text{S},(i-1)}\right). \tag{6}$$

The outermost positions of the spring $\varphi_{\text{S},0}$ and $\varphi_{\text{S},6}$ (which have no mass points in the model) follow from the equations:

$$\varphi_{\text{S},0} = \max(\quad \Phi_{\text{PS}},\ \varphi_{\text{DMF}} - \pi + \Phi_{\text{SS}},\ \varphi_{\text{S},1} - \Phi_{\text{nom},1}\ ) \tag{7}$$

$$\varphi_{\text{S},6} = \min(\ \pi - \Phi_{\text{PS}},\quad \varphi_{\text{DMF}} - \Phi_{\text{SS}},\ \varphi_{\text{S},5} + \Phi_{\text{nom},6}), \tag{8}$$

where Φ_{PS} is the half width of the primary stopper and Φ_{SS} is the half width of the secondary stopper, analogously (see Fig. 9). If the outermost spring elements are not compressed by a stopper, this choice of $\varphi_{\text{S},0}$ and $\varphi_{\text{S},6}$ will render the outermost spring elements idle. Depending on the min/max functions in the equations (7) and (8), the switching functions σ_1^{P}, σ_1^{S}, σ_6^{P} and σ_6^{S} can be calculated (see section IV-A).

1) Radial forces on the spring: For calculating the friction of the spring mass elements in the spring channel, it is required to calculate the radial forces $F_{\text{R},i}$ that act on these mass elements. Three different influences are considered for each of the mass elements ($i = 1 \dots 5$):

$$F_{\text{R},i} = F_{\text{centrifugal},i} + F_{\text{redirection},i} + F_{\text{bias},i}. \tag{9}$$

With an effective DMF radius r, the centrifugal force is simply found as ($i = 1 \dots 5$):

$$F_{\text{centrifugal},i} = m_i\, r \left(\dot{\varphi}_{\text{pri}} + \dot{\varphi}_{\text{S},i}\right)^2 \approx m_i\, r\, \dot{\varphi}_{\text{pri}}^2. \tag{10}$$

For each of the spring elements one can calculate a redirection force ($i = 1 \dots 6$):

$$F_{\text{S,defl},i} = \frac{T_{\text{S},i}}{r} \cdot 2\, n_{W,i} \sin\left(\frac{\varphi_{\text{F},i} - \varphi_{\text{F},(i-1)}}{2\, n_{W,i}}\right), \tag{11}$$

where $n_{W,i}$ is the number of coils of one spring element. Eqn. (11) slightly differs from the analogous expression given in [1]. These redirection forces $F_{\mathrm{S,defl},i}$ are recombined to the adjacent masses ($i = 2 \ldots 4$) with

$$F_{\mathrm{redirection},i} = \frac{1}{2} F_{\mathrm{S,defl},i} + \frac{1}{2} F_{\mathrm{S,defl},(i+1)}. \tag{12}$$

The redirection forces of the outermost springs, $F_{\mathrm{S,defl},1}$ and $F_{\mathrm{S,defl},6}$, are fully added to the forces which attack at the outermost masses, $F_{\mathrm{redirection},1}$ and $F_{\mathrm{redirection},5}$:

$$F_{\mathrm{redirection},1} = F_{\mathrm{S,defl},1} + \frac{1}{2} F_{\mathrm{S,defl},2}, \tag{13}$$

$$F_{\mathrm{redirection},5} = \frac{1}{2} F_{\mathrm{S,defl},5} + F_{\mathrm{S,defl},6}. \tag{14}$$

The bias term $F_{\mathrm{bias},i}$ models friction effects of an idle DMF [1]. It is set to:

$$F_{\mathrm{bias},i} = \begin{cases} F_{\mathrm{bias0}}, & i = 1 \ \vee \ i = 5 \\ 0, & \text{else.} \end{cases} \tag{15}$$

During our research F_{bias0} had to be chosen about two orders of magnitude larger than what [1] gave as a reference value.

2) Friction model: Now the spring friction can be deduced using the friction model:

$$T_{\mathrm{fric,max},i} = \mu\, r\, |F_{\mathrm{R},i}|, \tag{16}$$

with $\mu \approx 0.1$ being a coefficient of friction.

The friction $T_{\mathrm{fric},i}$ can be calculated using ($i = 1 \ldots 5$)

$$T_{\mathrm{fric},i} = \tag{17}$$
$$\begin{cases} T_{\mathrm{aff},i}, & \dot{\varphi}_{\mathrm{S},i} = 0 \ \wedge \ |T_{\mathrm{aff},i}| \leq \mu\, r\, |F_{\mathrm{R},i}| \\ \mu\, r\, |F_{\mathrm{R},i}| \operatorname{sgn}(T_{\mathrm{aff},i}), & \dot{\varphi}_{\mathrm{S},i} = 0 \ \wedge \ |T_{\mathrm{aff},i}| > \mu\, r\, |F_{\mathrm{R},i}| \\ \mu\, r\, |F_{\mathrm{R},i}| \operatorname{sgn}(\dot{\varphi}_{\mathrm{S},i}), & \text{else} \end{cases}$$

where $T_{\mathrm{aff},i}$ is the sum of both spring forces affecting one mass (see eq. 5). Calculating the friction $T_{\mathrm{aff},i}$ as shown in (IV-B.2) ensures that the friction always works against the direction of movement of each mass element.

To reach a complete standstill $\dot{\varphi}_{\mathrm{S},i} = 0$ in a numerical simulation, the Karnopp approach is used [9], [10] ($i = 1 \ldots 5$):

$$\dot{\varphi}_{\mathrm{S},i} = \begin{cases} 0, & |\dot{\varphi}_{\mathrm{S},i}| < \dot{\Phi}_{\min} \ \wedge \ |T_{\mathrm{aff},i}| \leq \mu\, r\, |F_{\mathrm{R},i}| \\ \dot{\varphi}_{\mathrm{S},i}, & \text{else} \end{cases}$$

C. Model parameters

Depending on the type of engine and clutch installed, table I contains reasonable parameters for a DMF model.

TABLE I
PARAMETERS FOR THE PRESENTED DMF MODEL.

Parameter	Magnitude		
Spring length	$\Phi_{\mathrm{nom},i}$	=	$\frac{1}{6}155°$
# of coils of a spring	$n_{W,i}$	=	$\frac{1}{6}45$
Spring radius	r	=	$0.15\,\mathrm{m}$
Primary stopper half width	Φ_{PS}	=	$10°$
Secondary stopper half width	Φ_{SS}	=	$6°$
Bias force	F_{bias0}	=	$500\,\mathrm{N}$
Sealing friction	$\lvert T_{\mathrm{seal}}\rvert$	=	$10\,\mathrm{Nm}$
Spring stiffness	c_i	=	$6 \cdot 500 \frac{\mathrm{Nm}}{\mathrm{rad}}$
Coefficient of friction	μ	=	0.1
Primary flywheel inertia	J_{pri}	=	$0.1\,\mathrm{kg\,m^2}$
Secondary flywheel inertia	J_{sec}	=	$0.01\,\mathrm{kg\,m^2}$
Spring mass	m_i	=	$\frac{1}{5}0.5\,\mathrm{kg}$
Spring inertia	$J_i = m_i\, r^2$	=	$0.002\,\mathrm{kg\,m^2}$

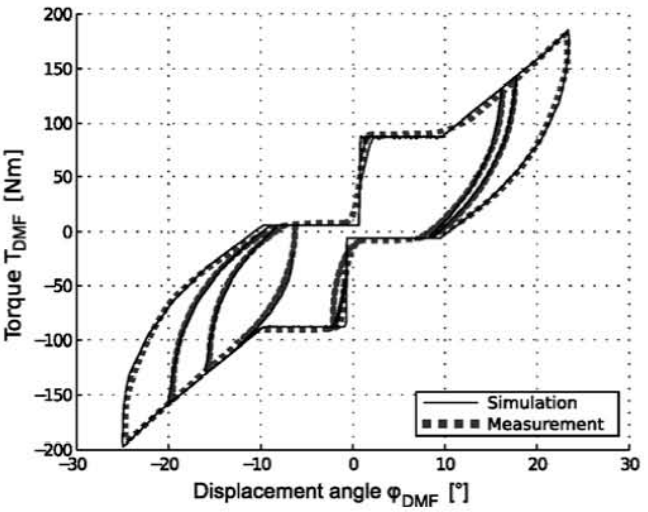

Fig. 11. Simulation of a few changes of load at about 2200 ¹/min. Measurement data from [1].

V. SIMULATION RESULTS

The model shown in the previous section can reproduce measurement data very well. All described physical effects can be simulated using the model. This includes the stiction effects at high engine speed levels (see Fig. 11) and the changing stiffness due to friction effects which depends on engine speed and transferred torque (see Fig. 12).

However, it must be noted that the measurement data which were used for validation have been taken from literature [1].

The presented model is implemented in MATLAB/SIMULINK. As the spring model is quite stiff, sample times around $h = 100\,\mu\mathrm{s}$ are required to ensure stable forward integration for engine stimulations up to 6000 ¹/min. $\dot{\Phi}_{\min} = 0.5\,\frac{\mathrm{rad}}{\mathrm{s}}$ was chosen as a lower speed bound in the Karnopp friction model.

VI. OBSERVABILITY

Since the springs are compressed once the DMF transmits torque from one flywheel to the other, the transmitted torque can be estimated from the spring length and the relative acceleration of one flywheel compared to the other one. Therefore the observability of the DMF depends on the stiffness of the connection between both flywheels: As long as a large angular displacement is required to transfer torque, the system is easily observable. At higher engine speeds however, the centrifugal forces will increase friction. As demonstrated in sections III and IV, this can be regarded as an increased spring stiffness: the DMF becomes is unobservable at higher engine speeds. One can intuitively understand this by looking at Fig. 7 which shows a step in the angle-torque graph at higher engine speeds. This resembles a rigid connection between both flywheels, or an infinite stiffness.

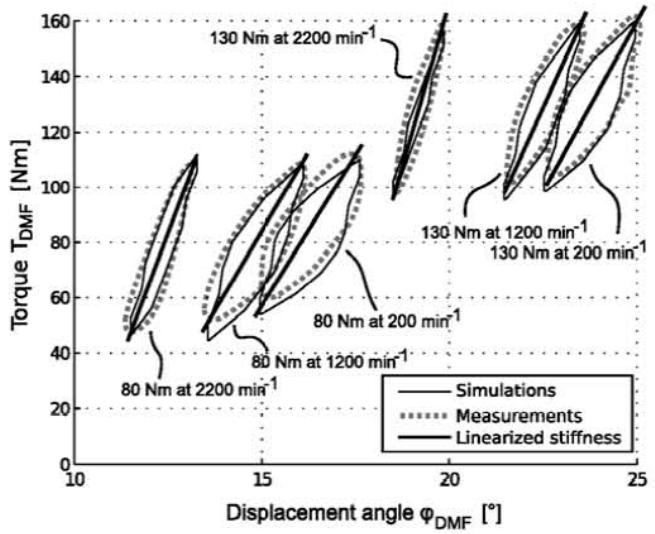

Fig. 12. Simulation of small displacement cycles at different torques and speeds. Measurement data from [1].

For estimating the DMF torque at low engine speeds, the following simplified model is proposed which neglects all nonlinear effects:

$$\dot{T}_{\text{eng}} = 0 \tag{18a}$$

$$\dot{T}_{\text{clu}} = 0 \tag{18b}$$

$$\ddot{\varphi}_{\text{DMF}} = -\frac{T_{\text{eng}}}{J_{\text{pri}}} - \frac{T_{\text{clu}}}{J_{\text{sec}}} - \left(\frac{1}{J_{\text{pri}}} + \frac{1}{J_{\text{sec}}}\right) c\, \varphi_{\text{DMF}} \tag{18c}$$

$$\ddot{\varphi}_{\text{pri}} = \frac{T_{\text{eng}}}{J_{\text{pri}}} + \frac{c\, \varphi_{\text{DMF}}}{J_{\text{pri}}}. \tag{18d}$$

Here φ_{DMF} represents the displacement angle of the DMF while $\dot{\varphi}_{\text{pri}}$ is the velocity of the primary flywheel (and $\dot{\varphi}_{\text{sec}} = \dot{\varphi}_{\text{DMF}} + \dot{\varphi}_{\text{pri}}$ therefore the velocity of the secondary flywheel). Both the angle φ_{DMF} and the angular velocities $\dot{\varphi}_{\text{pri}}$ and $\dot{\varphi}_{\text{sec}}$ are measurable. For generating continuous measurements from discrete shaft encoder signals, an event-triggered Kalman-Filter similar to [11] was used. T_{eng} and T_{clu} are the engine torque and the clutch torque. These are the states we are interested in. Just as in section IV, J_{pri} and J_{sec} represent inertias. c denotes a spring constant which can be derived by linearization of the main DMF model.

Since the model (18a)-(18d) is linear, a state observer could be constructed using an LQR approach. Fig. 13 shows the simulated launch phase of a 4-stroke diesel engine. For the simulation, the DMF model described in section IV was coupled with a complex engine model. Even with a conservative choice of the observer parameters, the simulated powertrain torque could be estimated.

VII. CONCLUSIONS

The Dual Mass Flywheel (DMF) has been presented as a device for oscillation dampening at low engine speeds. The main physical effects which affect the dynamic behavior have been identified. This mainly includes a spring model which shows hysteresis effects due to speed-dependent friction.

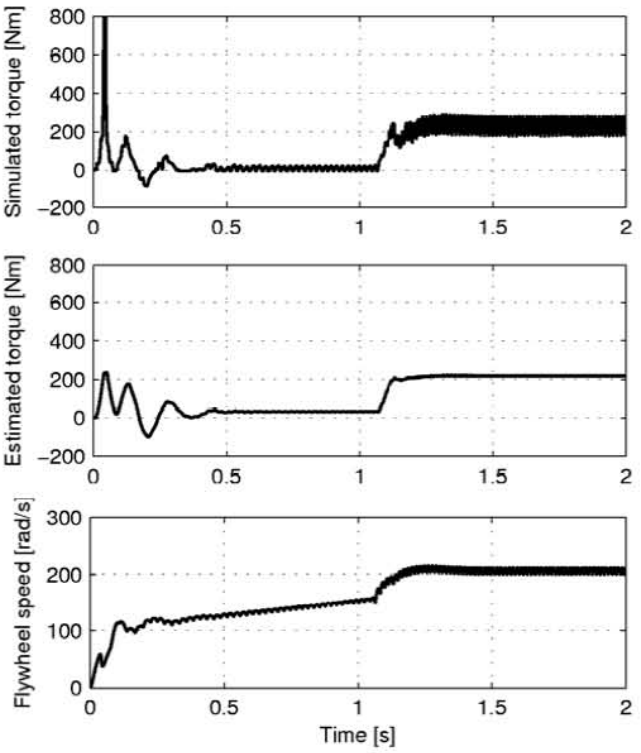

Fig. 13. Engine launch and driveaway simulation of a 4-stroke Diesel engine. Top: simulated torque T_{clu} (by complex model). Middle: estimated torque T_{clu} (by LQR observer). Bottom: simulated primary flywheel speed. (engine model: GETRAG).

Altogether, the DMF has been modeled as a nonlinear dynamic system with 14 states.

Once equipped with speed sensors, the DMF can be used as a torque estimator for advanced powertrain control tasks. For this application, a simplified linear DMF model has been proposed. A LQR torque observer has been deduced from this model which correctly observes the powertrain torque at low engine speeds. At higher engine speeds however, centrifugal forces will render the DMF unobservable.

REFERENCES

[1] Ralph Lux. *Ganzheitliche Antriebsstrangentwicklung durch Integration von Simulation und Versuch*. Disscrtation, Uni Karlsruhc, 2000.

[2] A. Albers and R. Lux et al. Integration of simulation and testing in power train engineering. In *testing expo*. Uni Karlsruhe, 2002.

[3] Albert Albers. Advanced Development of Dual Mass Flywheel (DMFW) Design. *LuK Symposium*, pages 1–38, 1994.

[4] A. Kooy, A. Gillmann, J. Jäckel, and M. Bosse. DMFW – Nothing New? *LuK Symposium*, pages 5–14, 2002.

[5] Wolfgang Reik. Höherer Komfort und weniger Geräusch durch das Zweimassenschwungrad. *ATZ*, 12:896–900, 1998.

[6] W. Reik, R. Seebacher, and A. Kooy. Dual Mass Flywheel. *LuK Symposium*, pages 69–93, 1998.

[7] A. Nicola and B. Sauer. Rotational Vibrometers Help Determine the Transmission Behavior of a DMF. *Polytec*, 4:14–15, 2007.

[8] A. Walter, U. Kiencke, S. Jones, and T. Winkler. Misfire Detection for Vehicles with Dual Mass Flywheel. *SAE Conference*, 2007.

[9] D. Karnopp. Computer simulation of stick-slip friction in mechanical dynamic systems. *ASME DSMC*, 107(1):100–103, 1985.

[10] J. Zimmermann, O. Sawodny, T. Hausotte, and G. Jäger. Friction modelling of a linear high-precision actuator. *IFAC*, 2005.

[11] Adam Lagerberg and Bo S. Egardt. Backlash gap position estimation in automotive powertrains. *7th European Control Conference*, 2003.